THE JOURNAL OF PHYSICAL CHEMISTRY C

Article

Cite This: J. Phys. Chem. C 2018, 122, 25059−25066

pubs.acs.org/JPCC

New Insights into the Multiexciton Dynamics in Phase-Pure Thick-Shell CdSe/CdS Quantum Dots

Lei Zhang,[†] Hao Li,[‡] Chen Liao,[†] Hongyu Yang,[†] Ruilin Xu,[†] Xiaoshun Jiang,*[,‡] Min Xiao,[‡] Changgui Lu,[†] Yiping Cui,[†] and Jiayu Zhang*[,†]

[†]Advanced Photonics Center, Southeast University, Nanjing 210096, Jiangsu, China

[‡]National Laboratory of Solid State Microstructures, College of Engineering and Applied Sciences, and School of Physics, Nanjing University, Nanjing 210093, China

Supporting Information

ABSTRACT: The multiexciton states in semiconductor quantum dots (QDs) have obtained increasing attention because of their extensive potential applications. Here, the pump-intensity-dependent multiexciton process in phase-pure wurtzite CdSe/CdS QDs is revealed by analyzing a fast photoluminescence (PL) decay component. The experimental results show that the PL decay traces can be fitted well by a superradiance decay function. The average number of excitons per QD ($\langle N \rangle$), obtained by fitting PL decay traces, is proportional to the power density, which is consistent with their theoretical calculations. However, the $\langle N \rangle$ starts to exhibit the saturation trends when the exciton number reaches about 6, which maybe result from the increased nonradiative losses of excitons at higher pump levels. The results give us deeper insights into the multiexciton dynamics process of CdSe/CdS QDs from the viewpoint of PL decay mechanism. Moreover, the fitting results are further confirmed by the multiband amplified stimulated emission measurements. Finally, we fabricate QD microlasers based on the microdisk resonator, indicating that CdSe/CdS QDs will be a promising lasing gain material for prospective applications in practical QD lasers.

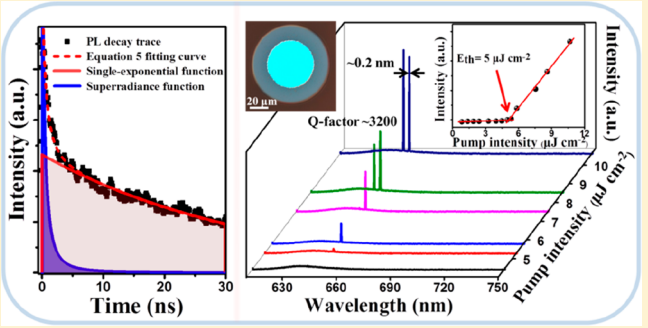

INTRODUCTION

Colloidal semiconductor quantum dots (QDs) have enormous potential applications in optical and optoelectronic devices owing to their distinctive quantum confinement effect.[1,2] Particularly, multiexciton states of QDs have attracted widespread attention in the aspect of carrier multiplication (CM) and optical gain.[3,4] However, the multiexciton decay becomes progressively faster as the number of excitons in QDs increases,[5] as expected for ultrafast nonradiative Auger recombination (AR), which has been proposed as the dominant nonradiative pathway for multiexciton relaxation.[6−8] The fast Auger decay would seriously limit the efficiency of CM[8,9] and the optical gain lifetime and bandwidth,[4,10] as well as even give rise to photoluminescence (PL) blinking in a single QD.[11,12] Thus, the Auger process severely restricts the further insights into the dynamics of higher-order excitons.

To solve this problem, a new type of phase-pure wurtzite (WZ) CdSe/CdS core/shell QDs provide new prospects to suppress nonradiative losses of excitons by enabling control over quantum confinement.[10,13−16] Because of the thick CdS shells and the partial spatial separation of exciton wave function, these QDs have been proven to efficiently inhibit AR and PL blinking.[15−18] Meanwhile, the relatively high epitaxial temperature and long reaction time for the CdS shell could contribute to form an alloyed interfacial layer with "smoothing" of the confinement potential.[18−20] Recent studies suggested that the graded interface could dramatically reduce Auger decay rates compared with those samples of a "sharp" core/shell interface, resulting in consistently longer biexciton lifetimes and lower lasing thresholds.[19−22] Notably, the phase-pure WZ CdSe/CdS QDs have no interfacial potential barrier in comparison with zinc-blende/WZ (ZB/WZ) CdSe/CdS QDs, hence greatly improving the exciton recombination efficiency of core states.[23,24] Moreover, the experiments showed that the crystal phase of the CdS shell could transform from ZB to WZ under photoannealing[24] or higher growth temperature.[25] This implies that the phase-pure WZ CdSe/CdS QDs would possess better stability in practical applications.

The multiexciton process in QDs was very different from the single exciton;[5−8,10] the corresponding decay dynamics of exciton states could be extracted by a simple subtractive procedure.[5] However, the concrete impact of multiexciton states on PL decay dynamics is still unclear in such complicated quantum-confined regime. The theoretical study indicated that the interaction of excitons in quantum well with

Received: August 10, 2018
Revised: October 2, 2018
Published: October 4, 2018

DOI: 10.1021/acs.jpcc.8b07787
J. Phys. Chem. C 2018, 122, 25059−25066

a radiation field could induce a macroscopic transition dipole moment, resulting in the rapid radiative decay of excitons.[26] Such cooperative radiance (superfluorescent and superradiance) of excitons could be observed under the strong ultrashort pulsed laser excitation.[27−30] For example, the superfluorescent phenomenon of biexcitons has been reported in an ensemble of CuCl QDs,[27] and the superradiance process of high-density Frenkel excitons was observed in an R-phycoerythrin single crystal.[28] On the other hand, the excitonic superradiance has also been observed from a single ZnO tetrapod nanostructure; the radiative decay rates scaled directly with the number of excitons.[29] In a single CdSe-based core/shell QD, the exciton recombination rates were related to the coupling effect between the exciton states and photon field that is known as the superradiance effect.[30] From the above, the exciton dynamics process in CdSe/CdS QDs maybe contains the contribution of the superradiance process similar to the case in atoms or molecules, especially for the fast decay component under the presence of multiexcitons. Hence, it is meaningful for optical gain and lasing applications to study the multiexciton process in such excellent QD materials. Particularly, a kind of hybrid structure that semiconductor nanomaterials coupled to a whispering-gallery mode (WGM) microcavity has been widely proposed to realize high-performance lasing operation.[31−33]

In this work, a series of phase-pure WZ CdSe/CdS QDs were synthesized by the successive ionic layer adsorption and reaction (SILAR) method. We investigate the multiexciton process in CdSe/CdS QDs with different shell thicknesses by fitting PL decay traces using a superradiance decay function for the first time, thus obtaining the relationships between the average number of excitons per QD ($\langle N\rangle$) and pump intensity. Furthermore, the ASE performance of CdSe/CdS QDs was studied as a further validation for fitting results. Finally, the QDs have been exploited as a gain medium to fabricate WGM microlasers that realized a high-efficiency lasing emission with a low threshold of ∼5 μJ cm^{-2}, and the Q-factor was as high as 3200.

EXPERIMENTAL SECTION

Synthesis of Phase-Pure WZ CdSe/CdS Core/Shell QDs. Phase-pure WZ CdSe/CdS core/shell QDs were synthesized in two steps: first, synthesis of WZ CdSe cores at 380 °C according to the literature procedure.[16] Then, the SILAR method was used to control the epitaxial growth of the CdS shell on the surface of CdSe cores at high temperatures (310 °C) (see the Supporting Information).

Material Characterization. The PL emission spectra were measured with an Edinburgh F900 luminescence spectrometer. The UV−vis absorption spectra were collected using a Shimadzu (UV3600) spectrophotometer. The single-exciton PL decay traces and time-resolved PL measurements were performed by an electrically triggered streak camera system (Hamamatsu C5680) in the QD solution, excited by a round femtosecond-pulsed laser at 400 nm. Transmission electron microscopy (TEM) and high-resolution TEM (HRTEM) images were performed on a FEI Tecnai G2 electron microscope with an acceleration voltage of 200 kV. The optical image was measured by a metallographic microscope (Olympus, BX51M). X-ray diffraction (XRD) patterns were acquired using an X-ray diffractometer (Bruker, D8-DISCOVER) with a Cu−Kα source.

Calculation of Absorption Cross Section. Under lower pump levels, the PL saturation curves of ensemble CdSe/CdS QDs can be fitted with a function $\propto 1 - e^{-\langle N\rangle} = 1 - e^{-j\sigma}$, where j and σ is the laser pump fluence and the absorption cross section, respectively. The laser pump fluence j can be calculated from $j = P/EF$, where P is the laser power density, E is the laser repetition rate of 1 kHz, and F is the laser photon energy at 400 nm. According to the above relationships, we can obtain the theoretical function that $\langle N\rangle = j\sigma = \sigma P/EF$. Therefore, there is a linear relationship between $\langle N\rangle$ and P, and the σ/EF can be seen as their linear slope (δ).

Superradiance Decay Function and the PL Decay Fitting Function. The superradiance process of N atoms can be expressed as[34]

$$\frac{dX}{dt} = -\alpha X - \beta X^2 \tag{1}$$

where $X(t)$ is the atomic population in high-energy states and α and β is the coefficient of spontaneous emission and superradiance emission, respectively. When $t = 0$, N atoms are all in a high-energy state; the differential eq 1 has the following solution

$$X(t) = \frac{\alpha}{\gamma \exp(\alpha t) - \beta} \tag{2}$$

where

$$\gamma = \frac{\alpha + \beta N}{N} \tag{3}$$

The superradiance decay function can be derived from eq 2, and the radiation intensity formula: $I(t) = -h\nu\frac{dX}{dt}$, as shown in the following

$$I(t) = I_m \operatorname{csch}^2\left(\frac{t + \tau_d}{\tau_r}\right) \tag{4}$$

Here, csch is the hyperbolic cosecant function, I_m is the coefficient of superradiance intensity, τ_r is the decay time of the system, and τ_d is the delay time, where $I_m = \frac{(\gamma-\beta)^2}{4\beta}N^2$, $\tau_r = \frac{2}{(\gamma-\beta)N}$, and $\tau_d = \frac{1}{\alpha}\ln\frac{\gamma}{\beta}$. We can simplify them by eq 3 and then used for the simplification of superradiance decay function (eq 4), as shown below

$$I_m = \frac{(\gamma-\beta)^2}{4\beta}N^2 \to \frac{\alpha^2}{4\beta};\ \tau_r = \frac{2}{(\gamma-\beta)N} \to \frac{2}{\alpha};\ \tau_d = \frac{1}{\alpha}\ln\frac{\gamma}{\beta} \to \frac{1}{\alpha}\ln\left(\frac{\alpha}{N\beta} + 1\right)$$

Equation 4 simplified as:

$$I(t) = \operatorname{csch}^2\left(\frac{\alpha t}{2} + \frac{1}{2}\ln\left(\frac{\alpha}{N\beta} + 1\right)\right)$$

It is based on the fact that PL relaxation (long component) is controlled by single-exponential decay dynamics when all multiexcitons have already decayed.[35,36] Therefore, the PL decay fitting function could be expressed in the following equation

DOI: 10.1021/acs.jpcc.8b07787
J. Phys. Chem. C 2018, 122, 25059−25066

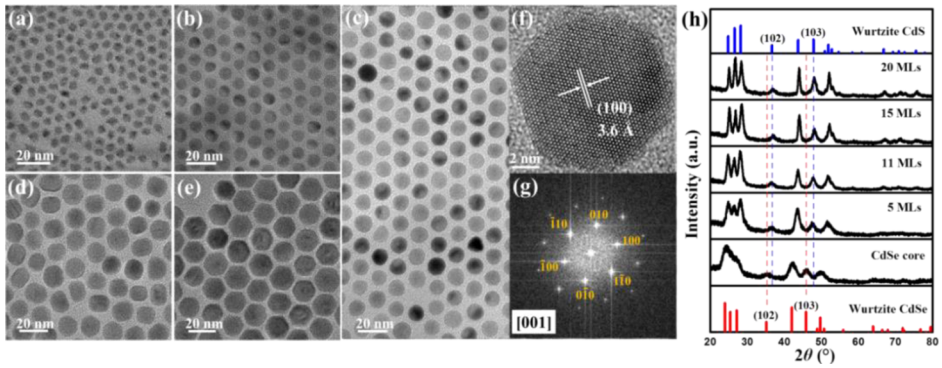

Figure 1. (a–e) TEM images of CdSe cores and their corresponding CdSe/CdS QDs with 5 MLs, 11 MLs, 15 MLs, and 20 MLs of the CdS shell, respectively. (f) HRTEM image of a CdSe/CdS QD (11 MLs) and the corresponding fast Fourier transform pattern (g) acquired along the zone axis [001]. (h) Typical XRD spectra of CdSe cores and CdSe/CdS QDs with the different shell thicknesses. Vertical lines indicate the standard peak positions of bulk WZ CdSe and CdS.

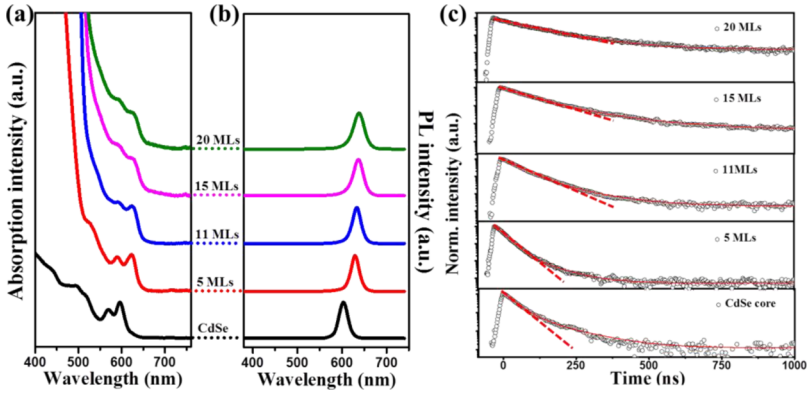

Figure 2. (a,b) Absorption and PL spectra of CdSe cores and CdSe/CdS core/shell QDs (5 MLs, 11 MLs, 15 MLs, and 20 MLs). (c) Single-exciton PL decay traces of CdSe cores and their corresponding CdSe/CdS QDs. The red solid lines stand for the bi-exponential fittings; the reduced χ^2 value is below 1.2. The red-dashed lines are added as the linear fitting curves for the initial data points, indicating the difference that fitted by single-exponential dynamics.

$$I(t) = I_m \operatorname{csch}^2\left(\frac{t + \tau_d}{\tau_r}\right) + B \exp(-\alpha t) + C \quad (5)$$

Here, α represents the reciprocal of single-exciton lifetime, the α values of CdSe/CdS QDs with 5 monolayers (MLs), 11 MLs, and 15 MLs of the CdS shell are 0.065, 0.0222, and 0.0106, respectively. In order to improve the goodness of the fit, the constant term C is added to reduce the interference from the baseline. In this paper, the PL decay traces are fitted by eq 5 through the Origin software. Finally, we can obtain the average number of excitons per QD by fitting PL decay traces using above α and the fitting optimal parameter β of 0.075, 0.08, and 0.083 for CdSe/CdS QDs (5 MLs, 11 MLs, and 15 MLs) sample, respectively.

ASE and Lasing Investigations. For ASE and lasing investigations, an amplified femtosecond Ti:sapphire laser system (Legend-F-1k; 800 nm, 1 kHz repetition rate, 100 fs pulse width) was used. The 400 nm beam was obtained from a β-barium borate crystal. The modal gain was characterized by the variable stripe length (VSL) measurement, and all samples used for VSL and ASE were of uniform and closed-packed QD film. The gain coefficients (g) were determined by the following formula: $I = A(e^{gL} - 1)/g$, where I is the ASE intensity that is dependent on the excitation stripe length (L) and A is a constant proportional to the spontaneous emission intensity. The pump intensity was adopted to be three times the corresponding ASE threshold. For ASE measurements, a stripe pump was acquired using a cylindrical lens (10 cm focal length); the pulse energy could be continuously adjusted using a polarization filter. The stripe pump pulses were perpendicular to the film, and then the edge emitted beam was collected from the lateral parallel to the films by a fast optical multichannel analyzer (OMA, SpectraPro-300i). For lasing measurements, the silica-based microdisk was constructed on silicon chips (with 40 μm radius and 2 μm thickness), the incident laser pulse (400 nm) was focused onto the microdisk resonator with a microscope objective (60×, NA = 0.65), and the exact position of excitation spot was observed by a CCD camera. The lasing emission spectra were monitored via OMA.

RESULTS AND DISCUSSION

Morphology and Crystal Structure Characterization. Figure 1a–e shows the TEM images of WZ CdSe cores and a series of CdSe/CdS core/shell QDs. The average particle diameter increases from 4.3 ± 0.4 to 18.3 ± 0.7 nm with the CdS shell growth, which corresponds to 20 MLs (1 ML = 0.35 nm) of the CdS shell. The crystal structure of CdSe/CdS QDs (11 MLs) was carried out via HRTEM imaging. Figure 1f,g shows a measured lattice distance of 3.6 Å, which is associated with the (100) planes of WZ CdS. Further, the WZ structure of these CdSe cores and CdSe/CdS QDs at different shell growth stages is confirmed by XRD patterns (Figure 1h) with

DOI: 10.1021/acs.jpcc.8b07787
J. Phys. Chem. C 2018, 122, 25059–25066

the characteristic (102) and (103) Bragg peaks. As the shell thickness increased, the peak positions were shifted from bulk WZ CdSe (red vertical lines) to WZ CdS (blue vertical lines) accompanied by a narrowing of diffraction peaks, which demonstrated the epitaxial WZ CdS shell formations on WZ CdSe cores. We believe that the slow shell growth at high temperatures (310 °C) conduced to keep the original WZ structure of the starting core material. Besides, the interdiffusion of anions at the core/shell interface could result in an interfacial alloying layer with a smoothed confinement potential.[18−20] The gradient interface not only provides more complete healing of strain-induced defects[37] but also further availably alleviates the Auger effect.[19−22] Therefore, such potential defect-free CdSe/CdS QDs would significantly contribute to decrease the nonradiative losses of excitons.

Optical Properties. Absorption and PL spectra of CdSe cores and CdSe/CdS core/shell QDs are shown in Figure 2a,b, respectively. Both the absorption and PL peaks have red shift with increasing shell thickness, as a consequence of a leakage of electron wave function into the shell.[19] PL quantum yield (QY) measurements (Figure S1a) show that the QYs rapidly increase with the CdS shell growth toward 11 MLs, which is observed to be as high as ∼90 ± 2%, consistent with that of previously reported phase-pure CdSe/CdS QDs.[16,18] Figure 2c shows their corresponding time-resolved PL decay traces. The PL decay traces could be fitted well by a bi-exponential function as reported in the literature,[19,25,38,39] which was also gradually inclined to be fitted with a single-exponential function in thick-shell QDs (red-dashed lines), indicating that the nonradiative process of a single exciton involving in surface or interfacial defects was better suppressed with the increasing shell thickness.[35,39] The average lifetimes of CdSe/CdS QDs with 20 MLs of the CdS shell (160 ns) are evidently longer than that of core-only CdSe QDs (15 ns) because of the reduced overlap of the electron−hole wave function,[15,40] whereby the electrons are delocalized into the CdS shell, whereas the holes remain primarily confined to the CdSe core region. Long PL lifetime is commonly observed in such spherical giant QDs, with a final lifetime reaching 200−300 ns.[39] To our knowledge, the delocalization of electron wave function could reduce Coulomb interactions between electrons and holes and further lower Auger losses.[10,13,41] In our previous works, giant CdSe/CdS QDs revealed more than 3 orders of magnitude decrease in AR rates,[18,35] thus enabling a superior gain performance.

Multiexciton Dynamics. The intrinsic mechanism for the generation of excitons is associated with the potential optical absorption ability of thick shells because of the direct correlation between the absorption cross section and the number of absorbed photons. We first estimated the absorption cross section of the QD sample. The PL intensity of CdSe/CdS QDs (5 MLs, 11 MLs, and 15 MLs) with increasing laser power density has been measured under lower pump levels (Figures 3a and S1b,c). The excitation intensity-dependent PL saturation curves could be fitted with a function $\propto 1 - e^{-j\sigma}$,[42] where j and σ is the laser pump fluence and the absorption cross section at the excitation wavelength, respectively. Thus, the average absorption cross section of CdSe/CdS QDs with 5 MLs, 11 MLs, and 15 MLs of the CdS shell is $\sim(3.3 \pm 0.18) \times 10^{-14}$, $\sim(7.9 \pm 0.2) \times 10^{-14}$, and $\sim(1.6 \pm 0.25) \times 10^{-13}$ cm^2, respectively, suggesting that the σ value is increased with the thickness of the CdS shell. Compared to the absorption cross section of core-only CdSe QDs that are usually around 5.5×10^{-15} cm^2,[43] the σ value [$\sim(1.6 \pm 0.25) \times 10^{-13}$ cm^2] measured here for CdSe/CdS QDs (15 MLs) is enhanced by at least one order of magnitude, indicating that the high absorption cross section stems from the intrinsically excellent optical absorption capacity of the CdS shell. Hence, it benefits to produce substantial photogenerated excitons in the shell region, which could fast (a few picoseconds) relax into the CdSe cores.[44]

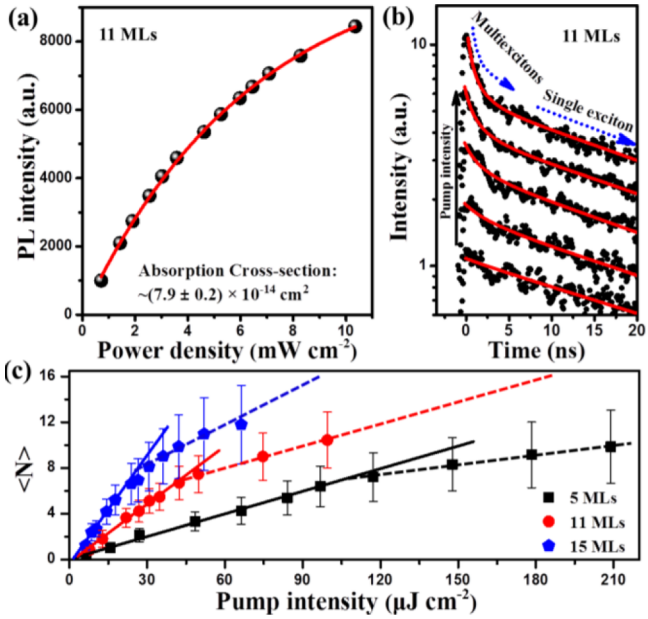

Figure 3. (a) PL intensity of CdSe/CdS QDs (11 MLs) measured with increasing laser power density (P) and fitted with the function $\propto 1 - e^{-\delta P}$, where δ is a fitting constant related to the absorption cross section (see Experimental Section). (b) Time-resolved PL decay traces of CdSe/CdS QDs (11 MLs) excited at 400 nm under varying pump intensities. The red solid lines show the fitting curves by eq 5. (c) Average number of excitons per particle ($\langle N \rangle$) as a function of pump intensity measured for CdSe/CdS QDs (5 MLs, 11 MLs, and 15 MLs), which is derived by fitting corresponding PL decay traces using eq 5. The solid lines are on behalf of their theoretical relationships. The dashed lines denote the variation trend of the number of higher-order excitons at higher pump intensities.

The exciton dynamics was directly involved in the PL decay process; thus, the time-resolved PL measurements were performed in the QD sample by a streak camera. Figure 3b shows the PL decay traces of CdSe/CdS QDs (11 MLs). Under low pump intensities, we can see that the PL decay of those QDs is operated by relatively slow single-exciton recombination. As the excitation intensity increases, an apparently fast decay component emerges in the first several nanoseconds, corresponding to the fast multiexciton decay.[10,35] The emission spectra (0−1 ns) show that the emission intensity was increased with the pump intensity, indicating that the fast decay component was mainly dominated by a robust radiative recombination process rather than the nonradiative decay process (Figure S2). Furthermore, the emission intensity (I_e) of CdSe/CdS QDs (11 MLs) was near exponentially proportional to the square of power density (I_p): $I_e \propto I_p^{2.17}$. (Figure S3), which is similar to the peculiarity of exciton superradiance.[29] According to the previous reports,[30] the fast exciton decay was related to the excitonic superradiance effect in QDs. Therefore, we speculate that the fast multiexciton decay may be also stemmed from the superradiance effect

DOI: 10.1021/acs.jpcc.8b07787
J. Phys. Chem. C 2018, 122, 25059−25066

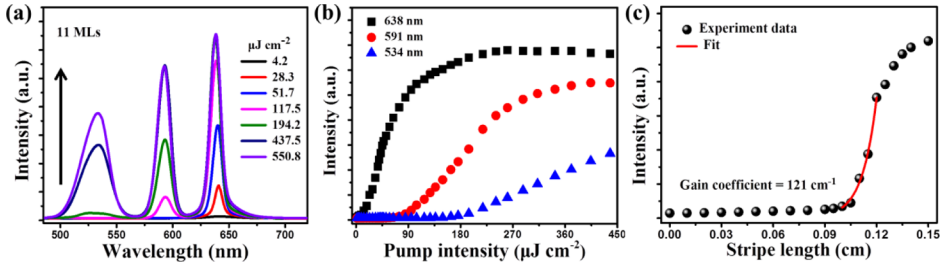

Figure 4. (a) ASE spectra from a close-packed CdSe/CdS QD (11 MLs) film under stripe femtosecond-pulsed excitation at 400 nm (1 kHz, 100 fs), measured with increasing pump intensities. (b) Emission intensity vs pump intensity curves for the three ASE peaks shown in (a). (c) VSL measurement for the CdSe/CdS QD (11 MLs) film. Fitting the data yields a gain coefficient of 121 cm^{-1}.

similar to the case in the atom system. Here, we put forward a method to analyze the multiexciton process by fitting PL decay traces using a PL decay fitting function (eq 5) (see Experimental Section). The PL decay traces can be fitted well by eq 5, as shown in Figure 3b. The adjusted R^2 value is about 0.99 (Figure S4), indicating very high fidelity of the fitting procedure. The fitting range is appropriate because the contribution of fast decay component gets negligible after 10 ns. Finally, Figure 3c shows the $\langle N \rangle$ value as a function of pump intensity for CdSe/CdS QDs with the 5 MLs, 11 MLs, and 15 MLs of the CdS shell, which is obtained by fitting corresponding PL decay traces using eq 5.

In theory, the relationships between $\langle N \rangle$ and power density P should satisfy the formula $\langle N \rangle = \sigma P/EF$ (see Experimental Section), where E is the laser repetition rate of 1 kHz, F is the laser photon energy at 400 nm, and σ used here is the above-obtained absorption cross section. Here, σ/EF can be seen as the linear slope of the theoretical formula. Therefore, the solid lines in Figure 3c represent the theoretical relationships between $\langle N \rangle$ and P. For all of the samples, there was a common characteristic that the $\langle N \rangle$ value was proportional to P within a certain range of pump intensity. At the same time, the data points were almost in perfect conformity with their own theoretical linear relationships, indicating that the research approach was correct. When the pump intensity continued to increase, the average number of excitons in QDs deviated from the theoretical values and started to exhibit different saturation trends (dashed lines in Figure 3c). The $\langle N \rangle$ value for all QD samples was up to about 6 before the appearance of exciton saturation phenomenon and finally larger than 10 with further increasing pump intensities, which could be indeed produced in these core/shell QDs.[10,45] The saturation effect results from photobleaching under very strong optical pumping, which is associated with the nonradiative losses of multiexcitons, for instance, the rapid scaling of AR rates with the number of excitons[4−8] and the increased electron trapping probability in the shell region as a consequence of strong electron delocalization with the increasing shell thickness.[13,15] The above results reveal that the multiexciton process in the fast PL decay component is relevant to the shell thickness of QDs, and their decay dynamics is analogous to the superradiance decay process in the atom system. Consequently, it is demonstrated that the nonradiative losses of higher-order excitons can be efficiently suppressed in such core/shell QDs and thus in favor of accumulating high-density excitons, which is sufficient to realize population inversion in core-based states for achieving high-efficiency ASE.

ASE Measurements from CdSe/CdS QDs. In order to further verify the above fitting results, we here measure the ASE performance of CdSe/CdS QDs (11 MLs) under the stripe modal confined optical pumping, as shown in Figure 4a. With the increasing pump intensity, the output emission from the film edge showed an obvious transition from spontaneous emission to ASE (1S) with the characteristics of spectral narrowing [full width at half-maximum (fwhm) ≈ 8−9 nm]. When the pump intensities further increased, two shorter-wavelength ASE peaks (at 591 and 534 nm) could also be detected, which involves the second (1P) and third (1D) quantization states, respectively.[10,18,24] The extension of optical amplification bandwidth to higher energies was due to excitonic state filling, which was only possible through the involvement of higher-order multiexcitons.[10] According to a simple particle in-a-box model, a population inversion of the first, second, and third electron quantized levels could be realized only for N at least 2, 6, and 14, respectively.[10,45] Actually, the number of excitons for the realization of ASE should be slightly larger than population inversion. As shown in Figure 4b, there is a superlinear dependence on the pump intensity with the clear threshold behavior for three ASE peaks. The ASE threshold for the first quantized level was only 15 μJ cm^{-2}. On the basis of the relationships between the $\langle N \rangle$ and pump intensity in Figure 3c, it was about two excitons (±0.5) generated in CdSe/CdS QDs near 1S ASE threshold, which was corresponded to the theory.[10,45] The ASE threshold for the second and third quantized levels was measured as 65 and 180 μJ cm^{-2}, respectively. In the same way, the corresponding $\langle N \rangle$ in CdSe/CdS QDs (11 MLs) was ∼7.6 ± 1.6 and ∼15.8 ± 2.4 at the pump levels near 1P and 1D ASE thresholds, respectively, which was also reasonable in comparison with the theoretical model. In addition, Figure 4c shows that the modal gain coefficient of CdSe/CdS QDs is acquired to be 121 cm^{-1} at the first stimulated emission peak,[46] indicating that the phase-pure thick-shell CdSe/CdS QDs possess outstanding ASE performance.

WGM Laser Performance. The robust multiexciton process and superior ASE performance indicate that thick-shell CdSe/CdS QDs can be an excellent lasing gain material. Here, we fabricate QD microlasers directly by spin-coating CdSe/CdS QD (11 MLs) solution on a microdisk resonator. Figure 5a illustrates a schematic diagram of the measurement system for QD microlasers, where the radius of the microdisk is about 40 μm. Figure 5b shows the emission spectra of QDs based on a microdisk cavity at lower excitation intensities (below the threshold). The modal spectra have the average free spectral range of 1.07 nm estimated near 648 nm by the equation of mode spacing (see the Supporting Information).

DOI: 10.1021/acs.jpcc.8b07787
J. Phys. Chem. C 2018, 122, 25059−25066

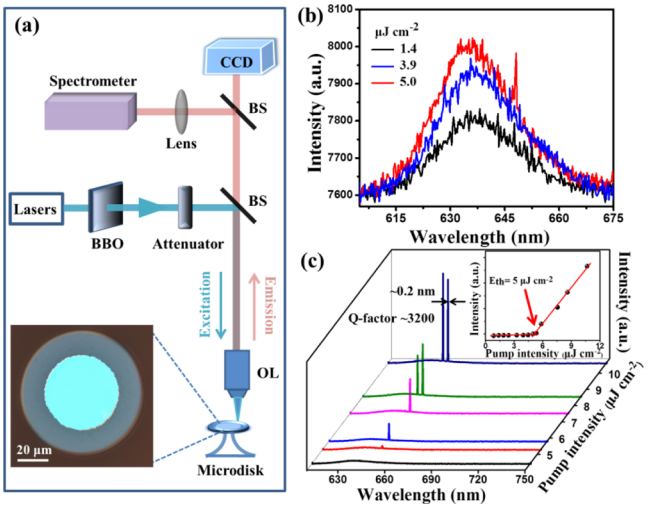

Figure 5. (a) Schematic diagram of the measurement system, where BBO, BS, and OL denote the frequency doubling crystal, beamsplitter, and objective lens, respectively. Inset: the top-view optical image of a typical microdisk cavity with a radius of 40 μm. (b) Emission spectra of CdSe/CdS QDs (11 MLs) on a microdisk cavity below the lasing threshold. (c) Lasing spectra of QD microlasers under different excitation intensities. Inset: the lasing emission intensity as a function of increasing pump intensities.

The lasing spectra of the QD microlasers under different excitation intensities are shown in Figure 5c. As the excitation intensity is above the threshold, a single-mode lasing emission was detected at the wavelength of 648 nm (fwhm ≈ 0.2 nm). When the excitation intensities were further increased, the multimode lasing emission started to appear, which might be from the mode with a higher threshold. The lasing action is unambiguously evidenced by spectral narrowing and a steep linear growth of lasing intensity, with a lasing threshold of ~5 μJ cm^{-2}, which is one of the lowest excitation thresholds (~2–10 μJ cm^{-2}) reported for QD lasers.[18,47] At the same time, the Q-factor of the microdisk coated with a QD film is estimated to be as high as 3200 by the equation $Q = \lambda/\Delta\lambda$, where λ and $\Delta\lambda$ are the lasing emission wavelength and fwhm, respectively. Hence, it is demonstrated that WGM QD lasers have the remarkable laser emission performance. The results are further proven that phase-pure thick-shell CdSe/CdS QDs have tremendous potential applications in the field of semiconductor QD microlasers.

CONCLUSIONS

In summary, the multiexciton process in phase-pure WZ CdSe/CdS QDs has been systematically investigated which is dependent on the pump intensity by fitting PL decay traces. We obtain the average exciton number of CdSe/CdS QDs (5 MLs, 11 MLs, and 15 MLs) under different pump intensities, which is consistent with their theoretical calculations before the exciton number reaching about 6. However, the exciton number trends slowly toward saturation with further increasing pump intensity, which may be induced by the increased nonradiative losses of excitons. At the same time, the ASE measurements of CdSe/CdS QDs (11 MLs) prove that the fitting results of $\langle N \rangle$ (2, 7.6, and 15.8) at the three ASE thresholds are basically conformed to the theory (2, 6, and 14), further indicating the correctness of the fitting scheme. These results give us more insights into the multiexciton states in the fast PL decay process and provide a new way from the view of superradiance mechanism to study the multiexciton dynamics of CdSe/CdS QDs. However, more experimental measurements are still needed in future works to determine whether this multiexciton dynamics process can be generally existed in other colloidal semiconductor nanomaterials. Finally, we have achieved a high-performance lasing emission from QD microlasers with an ultralow threshold and high Q-factor, demonstrating that the phase-pure CdSe/CdS QDs are going to be a superior gain medium for practical applications in laser devices.

ASSOCIATED CONTENT

Supporting Information

The Supporting Information is available free of charge on the ACS Publications website at DOI: 10.1021/acs.jpcc.8b07787.

Synthesis of phase-pure WZ CdSe/CdS QDs; PL QYs as a function of CdS shell thickness and absorption cross section of CdSe/CdS QDs (5 MLs and 15 MLs); emission spectra of CdSe/CdS QDs (11 MLs) in time range of 0–1 and 1–50 ns; relationships between emission intensity and power density for CdSe/CdS QDs (11 MLs); goodness of fit for tri-exponential function and eq 5; and calculations of free spectral range for the QD microlasers (PDF)

AUTHOR INFORMATION

Corresponding Authors

*E-mail: jxs@nju.edu.cn (X.J.).
*E-mail: jyzhang@seu.edu.cn (J.Z.).

ORCID

Yiping Cui: 0000-0002-4648-2506
Jiayu Zhang: 0000-0001-7868-6346

Notes

The authors declare no competing financial interest.

ACKNOWLEDGMENTS

This work was supported by the National Basic Research Program of China (973 Program, 2015CB352002), the Postgraduate Research & Practice Innovation Program of Jiangsu Province (KYCX17_0064), the Fundamental Research Funds for the Central Universities (2242017K41009, 2242018K41021), the Science and Technology Support Program of Jiangsu Province (BE2018117, BE2016021), and the Scientific Research Foundation of Graduate School of Southeast University.

REFERENCES

(1) Dai, X.; Zhang, Z.; Jin, Y.; Niu, Y.; Cao, H.; Liang, X.; Chen, L.; Wang, J.; Peng, X. Solution-processed, high-performance light-emitting diodes based on quantum dots. *Nature* **2014**, *515*, 96–99.
(2) Todescato, F.; Fortunati, I.; Gardin, S.; Garbin, E.; Collini, E.; Bozio, R.; Jasieniak, J. J.; Della Giustina, G.; Brusatin, G.; Toffanin, S.; et al. Soft-Lithographed Up-Converted Distributed Feedback Visible Lasers Based on CdSe-CdZnS-ZnS Quantum Dots. *Adv. Funct. Mater.* **2012**, *22*, 337–344.
(3) Schaller, R. D.; Agranovich, V. M.; Klimov, V. I. High-Efficiency Carrier Multiplication through Direct Photogeneration of Multi-Excitons via Virtual Single-Exciton States. *Nat. Phys.* **2005**, *1*, 189–194.
(4) Klimov, V. I.; Mikhailovsky, A. A.; Xu, S.; Malko, A.; Hollingsworth, J. A.; Leatherdale, C. A.; Eisler, H.-J.; Bawendi, M.

DOI: 10.1021/acs.jpcc.8b07787
J. Phys. Chem. C 2018, 122, 25059–25066

G. Optical Gain and Stimulated Emission in Nanocrystal Quantum Dots. *Science* **2000**, *290*, 314−317.
(5) Klimov, V. I.; Mikhailovsky, A. A.; McBranch, D. W.; Leatherdale, C. A.; Bawendi, M. G. Quantization of Multiparticle Auger Rates in Semiconductor Quantum Dots. *Science* **2000**, *287*, 1011−1013.
(6) Klimov, V. I. Optical Nonlinearities and Ultrafast Carrier Dynamics in Semiconductor Nanocrystals. *J. Phys. Chem. B* **2000**, *104*, 6112−6123.
(7) Achermann, M.; Hollingsworth, J. A.; Klimov, V. I. Multiexcitons Confined within a Subexcitonic Volume: Spectroscopic and Dynamical Signatures of Neutral and Charged Biexcitons in Ultrasmall Semiconductor Nanocrystals. *Phys. Rev. B: Condens. Matter Mater. Phys.* **2003**, *68*, 245302.
(8) Klimov, V. I.; McGuire, J. A.; Schaller, R. D.; Rupasov, V. I. Scaling of Multiexciton Lifetimes in Semiconductor Nanocrystals. *Phys. Rev. B* **2008**, *77*, 195324.
(9) Schaller, R. D.; Klimov, V. I. High Efficiency Carrier Multiplication in PbSe Nanocrystals: Implications for Solar Energy Conversion. *Phys. Rev. Lett.* **2004**, *92*, 186601.
(10) García-Santamaría, F.; Chen, Y.; Vela, J.; Schaller, R. D.; Hollingsworth, J. A.; Klimov, V. I. Suppressed Auger Recombination in "Giant" Nanocrystals Boosts Optical Gain Performance. *Nano Lett.* **2009**, *9*, 3482−3488.
(11) Kuno, M.; Fromm, D. P.; Hamann, H. F.; Gallagher, A.; Nesbitt, D. J. "On"/"Off" Fluorescence Intermittency of Single Semiconductor Quantum Dots. *J. Chem. Phys.* **2001**, *115*, 1028−1040.
(12) Nirmal, M.; Dabbousi, B. O.; Bawendi, M. G.; Macklin, J. J.; Trautman, J. K.; Harris, T. D.; Brus, L. E. Fluorescence Intermittency in Single Cadmium Selenide Nanocrystals. *Nature* **1996**, *383*, 802−804.
(13) Rabouw, F. T.; Lunnemann, P.; van Dijk-Moes, R. J. A.; Frimmer, M.; Pietra, F.; Koenderink, A. F.; Vanmaekelbergh, D. Reduced Auger Recombination in Single CdSe/CdS Nanorods by One-Dimensional Electron Delocalization. *Nano Lett.* **2013**, *13*, 4884−4892.
(14) She, C.; Fedin, I.; Dolzhnikov, D. S.; Dahlberg, P. D.; Engel, G. S.; Schaller, R. D.; Talapin, D. V. Red, Yellow, Green, and Blue Amplified Spontaneous Emission and Lasing Using Colloidal CdSe Nanoplatelets. *ACS Nano* **2015**, *9*, 9475−9485.
(15) Christodoulou, S.; Vaccaro, G.; Pinchetti, V.; De Donato, F.; Grim, J. Q.; Casu, A.; Genovese, A.; Vicidomini, G.; Diaspro, A.; Brovelli, S.; et al. Synthesis of Highly Luminescent Wurtzite CdSe/CdS Giant-Shell Nanocrystals Using a Fast Continuous Injection Route. *J. Mater. Chem. C* **2014**, *2*, 3439−3447.
(16) Chen, O.; Zhao, J.; Chauhan, V. P.; Cui, J.; Wong, C.; Harris, D. K.; Wei, H.; Han, H.-S.; Fukumura, D.; Jain, R. K.; et al. Compact High-Quality CdSe-CdS Core-Shell Nanocrystals with Narrow Emission Linewidths and Suppressed Blinking. *Nat. Mater.* **2013**, *12*, 445−451.
(17) Chen, Y.; Vela, J.; Htoon, H.; Casson, J. L.; Werder, D. J.; Bussian, D. A.; Klimov, V. I.; Hollingsworth, J. A. "Giant" Multishell CdSe Nanocrystal Quantum Dots with Suppressed Blinking. *J. Am. Chem. Soc.* **2008**, *130*, 5026−5027.
(18) Liao, C.; Xu, R.; Xu, Y.; Zhang, C.; Xiao, M.; Zhang, L.; Lu, C.; Cui, Y.; Zhang, J. Ultralow-Threshold Single-Mode Lasing from Phase-Pure CdSe/CdS Core/Shell Quantum Dots. *J. Phys. Chem. Lett.* **2016**, *7*, 4968−4976.
(19) García-Santamaría, F.; Brovelli, S.; Viswanatha, R.; Hollingsworth, J. A.; Htoon, H.; Crooker, S. A.; Klimov, V. I. Breakdown of Volume Scaling in Auger Recombination in CdSe/CdS Heteronanocrystals: The Role of the Core-Shell Interface. *Nano Lett.* **2011**, *11*, 687−693.
(20) Beane, G. A.; Gong, K.; Kelley, D. F. Auger and Carrier Trapping Dynamics in Core/Shell Quantum Dots Having Sharp and Alloyed Interfaces. *ACS Nano* **2016**, *10*, 3755−3765.
(21) Cragg, G. E.; Efros, A. L. Suppression of Auger Processes in Confined Structures. *Nano Lett.* **2010**, *10*, 313−317.
(22) Park, Y.-S.; Bae, W. K.; Baker, T.; Lim, J.; Klimov, V. I. Effect of Auger Recombination on Lasing in Heterostructured Quantum Dots with Engineered Core/Shell Interfaces. *Nano Lett.* **2015**, *15*, 7319−7328.
(23) Pinchetti, V.; Meinardi, F.; Camellini, A.; Sirigu, G.; Christodoulou, S.; Bae, W. K.; De Donato, F.; Manna, L.; Zavelani-Rossi, M.; Moreels, I.; et al. Effect of Core/Shell Interface on Carrier Dynamics and Optical Gain Properties of Dual-Color Emitting CdSe/CdS Nanocrystals. *ACS Nano* **2016**, *10*, 6877−6887.
(24) Liao, C.; Fan, K.; Xu, R.; Zhang, H.; Lu, C.; Cui, Y.; Zhang, J. Laser-Annealing-Made Amplified Spontaneous Emission of "Giant" CdSe/CdS Core/Shell Nanocrystals Transferred from Bulk-Like Shell to Quantum-Confined Core. *Photonics Res.* **2015**, *3*, 200−205.
(25) Nan, W.; Niu, Y.; Qin, H.; Cui, F.; Yang, Y.; Lai, R.; Lin, W.; Peng, X. Crystal Structure Control of Zinc-Blende CdSe/CdS Core/Shell Nanocrystals: Synthesis and Structure-Dependent Optical Properties. *J. Am. Chem. Soc.* **2012**, *134*, 19685−19693.
(26) Hanamura, E. Rapid Radiative Decay and Enhanced Optical Nonlinearity of Excitons in a Quantum Well. *Phys. Rev. B* **1988**, *38*, 1228−1234.
(27) Miyajima, K.; Kagotani, Y.; Saito, S.; Ashida, M.; Itoh, T. Superfluorescent Pulsed Emission from Biexcitons in an Ensemble of Semiconductor Quantum Dots. *J. Phys.: Condens. Matter* **2009**, *21*, 195802.
(28) Wang, H. Z.; Zheng, X. G.; Zhao, F. L.; Gao, Z. L.; Yu, Z. X. Superradiance of High Density Frenkel Excitons at Room Temperature. *Phys. Rev. Lett.* **1995**, *74*, 4079−4082.
(29) Ding, C. R.; Lin, W.; Chen, B. C.; Zhao, F. L.; Dong, J. W.; Shi, M.; Wang, H. Z.; Hsu, Y. F.; Djurišić, A. B. Super-Radiance of Excitons in a Single ZnO Nanostructure. *Appl. Phys. Lett.* **2008**, *93*, 151902.
(30) Bacher, G.; Weigand, R.; Seufert, J.; Kulakovskii, V. D.; Gippius, N. A.; Forchel, A.; Leonardi, K.; Hommel, D. Biexciton versus Exciton Lifetime in a Single Semiconductor Quantum Dot. *Phys. Rev. Lett.* **1999**, *83*, 4417−4420.
(31) Min, B.; Kim, S.; Okamoto, K.; Yang, L.; Scherer, A.; Atwater, H.; Vahala, K. Ultralow Threshold On-Chip Microcavity Nanocrystal Quantum Dot Lasers. *Appl. Phys. Lett.* **2006**, *89*, 191124.
(32) Wang, G.; Jiang, X.; Zhao, M.; Ma, Y.; Fan, H.; Yang, Q.; Tong, L.; Xiao, M. Microlaser Based on a Hybrid Structure of a Semiconductor Nanowire and a Silica Microdisk Cavity. *Opt. Express* **2012**, *20*, 29472−29478.
(33) Xie, W.; Stöferle, T.; Rainò, G.; Aubert, T.; Bisschop, S.; Zhu, Y.; Mahrt, R. F.; Geiregat, P.; Brainis, E.; Hens, Z.; et al. On-Chip Integrated Quantum-Dot-Silicon-Nitride Microdisk Lasers. *Adv. Mater.* **2017**, *29*, 1604866.
(34) Gu, Q. *Quantum Mechanics II*; Science press: Beijing, China, 2014.
(35) Zhang, L.; Liao, C.; Lv, B.; Wang, X.; Xiao, M.; Xu, R.; Yuan, Y.; Lu, C.; Cui, Y.; Zhang, J. Single-Mode Lasing from "Giant" CdSe/CdS Core-Shell Quantum Dots in Distributed Feedback Structures. *ACS Appl. Mater. Interfaces* **2017**, *9*, 13293−13303.
(36) Wu, K.; Lim, J.; Klimov, V. I. Superposition Principle in Auger Recombination of Charged and Neutral Multicarrier States in Semiconductor Quantum Dots. *ACS Nano* **2017**, *11*, 8437−8447.
(37) Morgan, D.; Gong, K.; Kelley, A. M.; Kelley, D. F. Biexciton Dynamics in Alloy Quantum Dots. *J. Phys. Chem. C* **2017**, *121*, 18307−18316.
(38) Bawendi, M. G.; Carroll, P. J.; Wilson, W. L.; Brus, L. E. Luminescence properties of CdSe quantum crystallites: Resonance between interior and surface localized states. *J. Chem. Phys.* **1992**, *96*, 946−954.
(39) Brovelli, S.; Schaller, R. D.; Crooker, S. A.; García-Santamaría, F.; Chen, Y.; Viswanatha, R.; Hollingsworth, J. A.; Htoon, H.; Klimov, V. I. Nano-Engineered Electron−Hole Exchange Interaction Controls Exciton Dynamics in Core−Shell Semiconductor Nanocrystals. *Nat. Commun.* **2011**, *2*, 280.
(40) Cihan, A. F.; Kelestemur, Y.; Guzelturk, B.; Yerli, O.; Kurum, U.; Yaglioglu, H. G.; Elmali, A.; Demir, H. V. Attractive versus

DOI: 10.1021/acs.jpcc.8b07787
J. Phys. Chem. C 2018, 122, 25059−25066

Repulsive Excitonic Interactions of Colloidal Quantum Dots Control Blue- to Red-Shifting (and Non-shifting) Amplified Spontaneous Emission. *J. Phys. Chem. Lett.* **2013**, *4*, 4146−4152.
(41) Spinicelli, P.; Buil, S.; Quélin, X.; Mahler, B.; Dubertret, B.; Hermier, J.-P. Bright and Grey States in CdSe-CdS Nanocrystals Exhibiting Strongly Reduced Blinking. *Phys. Rev. Lett.* **2009**, *102*, 136801.
(42) Hu, F.; Zhang, H.; Sun, C.; Yin, C.; Lv, B.; Zhang, C.; Yu, W. W.; Wang, X.; Zhang, Y.; Xiao, M. Superior Optical Properties of Perovskite Nanocrystals as Single Photon Emitters. *ACS Nano* **2015**, *9*, 12410−12416.
(43) Leatherdale, C. A.; Woo, W.-K.; Mikulec, F. V.; Bawendi, M. G. on the Absorption Cross Section of CdSe Nanocrystal Quantum Dots. *J. Phys. Chem. B* **2002**, *106*, 7619−7622.
(44) Zhu, H.; Song, N.; Rodríguez-Córdoba, W.; Lian, T. Wave Function Engineering for Efficient Extraction of up to Nineteen Electrons from One CdSe/CdS Quasi-Type II Quantum Dot. *J. Am. Chem. Soc.* **2012**, *134*, 4250−4257.
(45) Efros, A. L.; Efros, A. L. Interband Absorption of Light in a Semiconductor Sphere. *Semiconductors* **1982**, *16*, 772−775.
(46) Malko, A. V.; Mikhailovsky, A. A.; Petruska, M. A.; Hollingsworth, J. A.; Htoon, H.; Bawendi, M. G.; Klimov, V. I. From Amplified Spontaneous Emission to Microring Lasing using Nanocrystal Quantum Dot Solids. *Appl. Phys. Lett.* **2002**, *81*, 1303−1305.
(47) Di Stasio, F.; Grim, J. Q.; Lesnyak, V.; Rastogi, P.; Manna, L.; Moreels, I.; Krahne, R. Single-Mode Lasing from Colloidal Water-Soluble CdSe/CdS Quantum Dot-in-Rods. *Small* **2015**, *11*, 1328−1334.

DOI: 10.1021/acs.jpcc.8b07787
J. Phys. Chem. C 2018, 122, 25059−25066